Pergamon

*Int. J. Heat Mass Transfer.* Vol. 41, No. 12, pp. 1667–1679, 1998
© 1998 Elsevier Science Ltd. All rights reserved
Printed in Great Britain
0017–9310/98 $19.00+0.00

PII: S0017–9310(97)00289–5

# Onset and effects of instabilities from unstable stratification of density on mass transfer in channel shear layers at low Reynolds numbers

PHILLIP M. LIGRANI†
Convective Heat Transfer Laboratory, Department of Mechanical Engineering, University of Utah, Salt Lake City, UT 84112, U.S.A.

SUPRIYA GUPTA
Department of Chemical and Fuels Engineering, University of Utah, Salt Lake City, UT 84112, U.S.A.

and

J. CALVIN GIDDINGS‡
Field-Flow Fractionation Research Center, Department of Chemistry, University of Utah, Salt Lake City, UT 84112, U.S.A.

(*Received* 30 *September* 1996 *and in final form* 10 *September* 1997)

**Abstract**—The onset of mixing in the shear layer located between two coincident laminar streams of different velocity in a thin, ribbon-like channel is studied. Globally unstable density stratification is employed, which, with certain experimental conditions, results in augmented mixing and entrainment, and disruption of mass transfer of solid particles compared to channels with stable density gradients, and laminar, two-dimensional flow. The mixing onset boundary is quantified in terms of the Reynolds number, Richardson number, and channel flow rate ratios using a newly developed mixing onset parameter $R$. The results indicate that unstable density gradients, rather than shear gradients, are most responsible for inducing the mixing. © 1998 Elsevier Science Ltd. All rights reserved.

## INTRODUCTION

The present study focuses on the instabilities and mixing which develop from stratification of density in the shear layer between two coincident streams of different velocity. Much attention has been devoted to this and related areas to improve understanding of geophysical flows with shear-induced mixing [1–11], distribution of chemical pollutants in the atmospheric boundary layer [12–16], and non-premixed reacting and combusting flows [12–16].

The geophysical investigations are conducted directly in the ocean or other large bodies of water [1–5], or using laboratory experiments which scale the geophysical flows [6–11]. In the latter cases [6–11], a free shear layer is generally produced in a large open channel at high Reynolds numbers (i.e. from $10^2$–$10^3$) with a pressure gradient of approximately zero. The two streams are most often arranged with globally stable density gradients such that heavier fluid is located beneath the lighter fluid. The shear at the interface of the two streams is surrounded by uniform shear free flow creating the conditions for the development of Kelvin–Helmholtz instabilities. The resulting streamwise vortex tubes and Kelvin–Helmholtz rollers containing spanwise vorticity are both important in regard to mixing and entrainment between the two fluid streams. According to Schowalter *et al.* [11], density stratification not only alters the evolution of the streamwise vortex tubes, but also induces the development of an additional collection of vortex structures.

Komori *et al.* [12, 13], Nagata and Komori [14, 15], and Komori and Nagata [16] examine turbulent and molecular species diffusion across stratified mixing layers as applied to pollutant dispersal, and to chemi-

† Author to whom correspondence should be addressed.

‡ Distinguished Professor J. Calvin Giddings passed away on 24 October 1996 after a prolonged and courageous battle with cancer. Professor Giddings will always be remembered for his outstanding contributions in the areas of Chromatography and Separation Science. Of his numerous honors and awards, he received the ACS (American Chemical Society) Award in Chromatography and Electrophoresis, the ACS Award in Analytic Chemistry, the ACS Award in Separation Science and Technology, the Tswett Medal in Chromatography, and the Nichols Medal. He was twice nominated for the Nobel Prize in 1984 and 1992. Professor Giddings will also be remembered for his important contributions to the lives of the first two authors. We greatly miss our friend, colleague, and mentor.

## NOMENCLATURE

| | |
|---|---|
| $A_{stable}$ | area of retrieval plot under stable density gradient conditions |
| $A_{unstable}$ | area of retrieval plot under unstable density gradient conditions |
| $b$ | channel breadth |
| $d$ | particle diameter |
| $d_c$ | particle cut-off diameter, equation (3) |
| $F_a$ | fraction of particles retrieved from outlet $a$, equation (4) |
| $F_b$ | fraction of particles retrieved from outlet $b$, equation (5) |
| $l'$ | integral length scale characterizing vertical extent of mixing, equation (8) |
| $L$ | channel length |
| $R$ | mixing onset parameter, equation (11) |
| $Re$ | Reynolds number, equation (7) |
| $Ri$ | Richardson number, equation (6) |
| $s$ | sedimentation coefficient, equation (2) |
| $s'$ | channel streamwise coordinate measured from downstream edge of inlet splitter plate |
| $u$ | local streamwise velocity |
| $U$ | transfer particle sedimentation velocity, equation (1) |
| $U_c$ | spatially-averaged carrier velocity |
| $U_f$ | spatially-averaged feed velocity |
| $\dot{V}(a)$ | volumetric flow rate exiting outlet $a$ |
| $\dot{V}(a')$ | volumetric flow rate entering inlet $a'$ |
| $\dot{V}(b)$ | volumetric flow rate exiting outlet $b$ |
| $\dot{V}(b')$ | volumetric flow rate entering inlet $b'$ |
| $w$ | channel thickness |
| $x$ | channel streamwise coordinate |
| $z$ | channel traverse coordinate. |

Greek symbols

| | |
|---|---|
| $\Delta U$ | $U_c - U_f$ |
| $\Delta\rho$ | overall density difference between the feed and the carrier substreams, or local density difference, $\rho_f - \rho_c$ |
| $\eta$ | fluid viscosity |
| $\bar{\rho}$ | spatially-averaged density in all or part of the channel |
| $\rho_c$ | density of the carrier substream |
| $\rho_f$ | density of the feed substream |
| $\rho_p$ | particle density. |

cal and combustion reactions. Stable and unstable density gradients are investigated in homogeneous turbulence downstream of turbulence generating grids, generally without shear [12–16]. This is accomplished by introducing the two fluid streams at the same mean velocity. Some of these investigators' more recent research efforts focus on an experimental scheme to track instantaneous species concentrations [12], cross-correlations of species fluctuation concentrations in non-premixed homogeneous turbulence [13], differences between turbulence diffusions of active heat and passive mass gradients [14], Prandtl number effects [15], and effects of molecular diffusivities on turbulent heat and mass transfer [16].

The present work focuses on density stratification in shear layers as applied to the continuous separation of polystyrene latex particles ranging in size from 1–35 $\mu$m contained in a liquid stream (FL-70 detergent, sodium azide bacteriocide, and dissolved sucrose). The system employed is called a SPLITT channel and the process is referred to as SPLITT Fractionation or SF [17]. One such SF system is illustrated in Figs. 1(a) and 1(b). As shown, the channel is designed to split or separate two different flow substreams using splitter plates oriented in $x$–$z$ planes located at each end of the channel. SF is unique as it utilizes a powerful and generic strategy for rapid and continuous separation of particles with sizes as small as 0.01 $\mu$m and as large as 100 $\mu$m. By applying different kinds of fields or driving forces across the transverse direction of the laminar channel flow, particulate as well as macromolecular particles can be separated. To date, SF has been employed with a variety of different fields/gradients imposed in the transverse direction, such as gravitational, centrifugal, cross-flow, and concentration, to name a few [17]. In the present investigation, a gravitational field is employed because it works well for separation of particles larger than 1 $\mu$m.

Because our application is considerably different from that of other investigations of shear layers with density stratification [1–16], our channel and experimental set-up are also significantly different. In contrast to previous experiments which focused on geophysical phenomena [6–11], globally unstable density gradients are employed in the present study such that higher density fluid streams are located above the lower density streams (again, see Fig. 1). In addition, a streamwise pressure gradient is required in our enclosed channel, which is also relatively thin and ribbon-like with a thickness of 635 $\mu$m. The length is 20 cm and the breadth, $b$ is 4 cm, giving an aspect ratio of 63. Because of the relatively long and narrow inlet passages, both substreams are fully developed before they reach the downstream end of the inlet splitter plate just prior to initial shear layer formation.

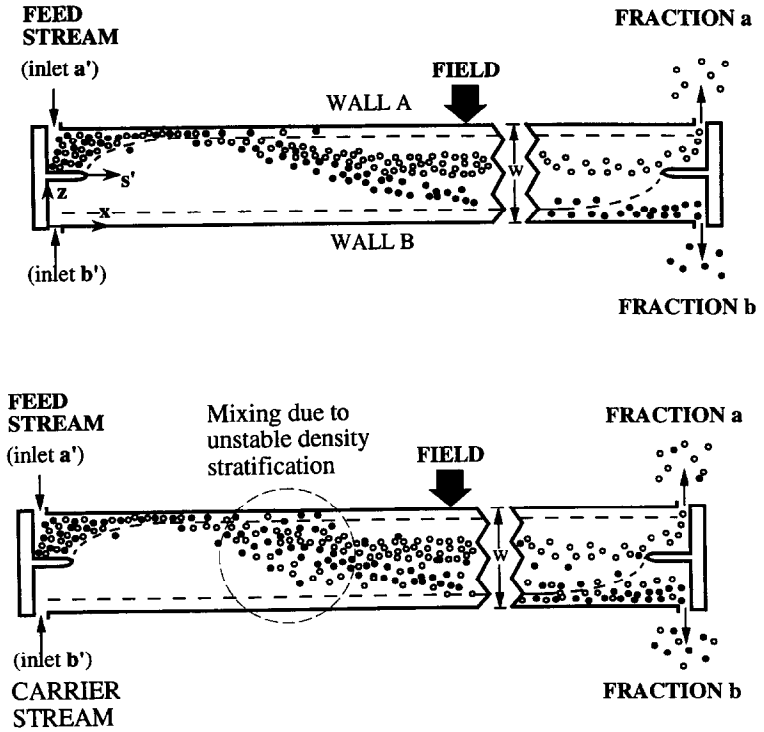


Fig. 1. Schematic of channel employed showing: (a) paths of polystyrene latex particles under nominal, stable operation, and (b) paths of polystyrene latex particles with mixing due to unstable density stratification.

In the other larger-scale geophysical studies mentioned [1–11], boundary layers are present prior to shear layer formation and uniform shear free flow is present outside of the shear layers. Our study is also considerably different from efforts described by Komori and co-workers [12–16], who generally investigate stably stratified mixing layers with homogeneous turbulence and no shear. In contrast, the flows in our channel are nominally laminar with significant shear, and stratification which is globally unstable, as mentioned.

The Reynolds numbers and Richardson numbers used in our study are compared to ones from several other studies [7, 9, 11] in Fig. 2. Also included are results from another 1.59 cm thick channel used for flow visualization [18]. *Re* and *Ri* values on the figure are from studies which employ density gradients which are both globally stable (open symbols, $\Delta\rho < 0$), and globally unstable (closed symbols, $\Delta\rho > 0$). Consequently, logarithms of absolute values of the Richardson number, *Ri*, are employed on the abscissa. No results from Komori and co-workers [12–16] are included in Fig. 2 since the flows they investigate generally contain no shear. Consequently, both $\Delta U$ and $l'$ are zero in those studies, which prevents meaningful calculation of the Richardson and Reynolds numbers employed in Fig. 2.

Figure 2 shows that our Reynolds numbers range

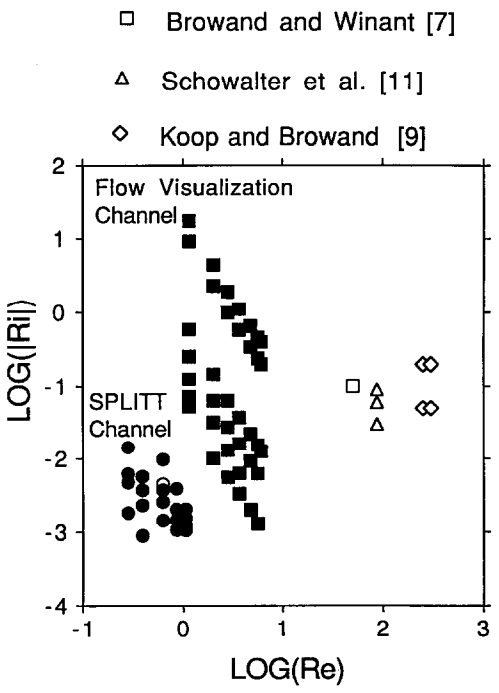


Fig. 2. Ranges of experimental parameters covered by the present study and by three other investigations. Open symbols: globally stable stratification ($\Delta\rho < 0, Ri < 0$). Closed symbols: globally unstable stratification ($\Delta\rho > 0, Ri > 0$).

from $10^{-1}$–$10^{1}$ which are significantly lower than values from three other studies [7, 9, 11], and absolute values of our Richardson numbers range from $10^{-3}$–$2 \times 10^{1}$ which cover the same range of values used in several other investigations [7, 9, 11]. The present data thus cover experimental conditions not previously investigated, thereby providing additional information on the relative importance of shear induced instabilities and instabilities due to density stratification. Our study is the first to aim at understanding the onset of instabilities and resulting mixing from density stratification with polystyrene latex particles in a thin, ribbon-like channel. Because the mixing onset boundary is established, the presence of substantial mixing in the channels employed in other applications can be determined when initial conditions, boundary conditions, Reynolds numbers, and Richardson numbers are similar. Knowledge of the mixing onset boundary also allows similar SF channels to be operated with adequate particle separation resolution and successful separations of different sizes of particles. Unstable channel operation can thus be avoided wherein nominal mass transfer mechanisms are disrupted by unwanted mixing and entrainment processes.

## BACKGROUND

Nominal mass transfer in an SF channel with stable, laminar, two-dimensional flow is illustrated by Fig. 1(a). The top inlet substream (or feed substream), denoted $a'$, contains the particles to be separated (in this case, polystyrene latex particles), and often has a higher density than the bottom inlet substream (or carrier substream), which is denoted $b'$. Inlet and exit flow rates in the channel are adjusted to produce laminar flow during nominal operation, and to give $\dot{V}(b') > \dot{V}(a')$ so that the top feed substream is compressed into a thin lamina close to wall $A$. Particle migration along the transverse direction is driven by a suitable field. In this study, gravity is employed, as mentioned. The velocity which ordinarily induces the mass transfer of the spherical particles from wall $A$ to wall $B$ in Fig. 1(a) is the sedimentation velocity $U$, given by

$$U = sG \tag{1}$$

where $G$ is the field induced acceleration due to gravity, and $s$ is the sedimentation coefficient, expressed using an equation of the form

$$s = \frac{(\rho_p - \rho_c)d^2}{18\eta}. \tag{2}$$

Thus, based on the magnitude of the driving force from the induced field and the frictional resistance experienced by different particles, they occupy different transverse positions while the axial channel flow displaces them towards the outlet end of the channel. Particles mobile enough to cross the second imaginary plane, termed the outlet splitting plane (OSP), exit outlet $b$. The rest exit outlet $a$, as shown in Fig. 1(a). The location of the outlet splitting plane is readily adjusted by regulating the inlet and outlet channel flow rates, $\dot{V}(a')$, $\dot{V}(b')$, $\dot{V}(a)$, and $\dot{V}(b)$ [17].

With nominal stable operation, setting the channel flow rates also sets the ranges of particle sizes which exit outlets $a$ and $b$ [17]. Under fixed flow conditions in an SF channel, particles smaller than a certain size $d_0$ exit entirely from outlet $a$, whereas ones larger than another size $d_1$ exit entirely from outlet $b$. The particles in between these two sizes ($d_1$–$d_0$) are not fully resolved and exit both outlets in different proportions. The specific diameter associated with the particle size which exits outlets $a$ and $b$ in equal proportions (i.e. 50% exits outlet $a$ and 50% exits outlet $b$) is referred to as the particle cut-off diameter $d_c$. It is given by [17]

$$d_c = \sqrt{\frac{18\eta(\dot{V}(a) - 0.5\dot{V}(a'))}{bL(\rho_p - \rho_f)G}}. \tag{3}$$

Thus, from equation (3), the cut-off diameter can be altered by changing the channel flow rates, $\dot{V}(a)$ and $\dot{V}(a')$. SF theory [17] further provides tools to determine the locations of particles of all sizes throughout the channel, provided the situation illustrated in Fig. 1(a) is present and the flow is entirely laminar, stable, and two-dimensional.

With mixing and/or entrainment in the channel, different sizes of particles are spread across the entire channel breadth as they are advected downstream, and the situation illustrated by Fig. 1(b) is present. When this occurs, particles of all sizes exit the channel through both outlets $a$ and $b$, and mass transfer across the channel thickness is considerably different compared to a channel with stable, laminar, two-dimensional flow. Consequently, different sizes of particles are not resolved, and little or no separation of different ranges of particle sizes occurs. Augmented mixing and/or entrainment can occur due to local turbulence, or development of any one of a variety of vortex structures. With the present experimental arrangement, $\Delta\rho > 0$ and fluid densities are higher in the feed stream than in the carrier substream (except for one baseline set of results wherein $\Delta\rho < 0$). The amount of mixing of all sizes of particles at outlets $a$ and $b$ is strongly tied to the normalized magnitude of $\Delta\rho$, the difference in density between these two inlet substreams. The onset of such mixing and entrainment, and the characterization in terms of this density difference, are the primary focus of this study.

## EXPERIMENTAL APPARATUS AND PROCEDURES

### *The channel*

The channel inlets are supplied by two reservoirs 6000 ml (carrier substream) and 100 ml (feed substream) in size, which allow the facility to be operated continuously for up to 135 min. The splitter plates

span the entire channel breadth at each end (channel dimensions: $L = 20$ cm, $b = 4.0$ cm, and $w = 635$ $\mu$m). Each splitter plate is made of stainless steel and is 127 $\mu$m thick and 8 cm long. Ends are machined to be flat with sharp corners. At the inlet, the splitter plate and channel walls provide a development length of 159 hydraulic diameters which is sufficient to produce fully developed channel flows at the downstream edge of the splitter plate. The inlet feed substream to the channel is pumped using a Gilson Inc. miniplus peristaltic pump, which provides 0.75 ml/min to inlet $a'$. A FMI Inc. QD-0 peristaltic pump provides 5–21 mL/min to supply the carrier substream at inlet $b'$. The flow rates at the two outlets denoted $a$ and $b$ are controlled by adjusting the back pressure in the flow lines.

*Fluid stream characteristics*

The fluid used at both channel inlets (feed and carrier substreams) is an aqueous solution of 0.1% weight by volume of FL-70 detergent and 0.02% weight by volume of sodium azide bacteriocide. Polystyrene latex particles with nominal diameters ranging in size from 1–35 $\mu$m and density of 1.05 g/ml are additionally employed in the feed substream. The density of the feed ($\rho_f$) and/or carrier ($\rho_c$) substreams is modified by adding sucrose crystals dissolved in water to vary the degree of stratification between the two substreams. The sucrose is added to the feed substream to produce unstable stratification ($\rho_f > \rho_c$) and to the carrier substream to produce stable stratification ($\rho_c > \rho_f$). The polystyrene latex particles are thus tracers which follow events in the flow and then indicate the nature of these events by their size distributions at the two channel outlets.

*Measurement of distributions of particle sizes*

Distributions of the sizes of the polystyrene latex particles at the exits of the channel are analyzed and measured using a FFFractionation Inc. model S101 sedimentation field-flow fractionation (SdFFF) system. This is a particle separation and characterization technique which works well for such analysis [19]. To accomplish the sizing, the sample is first injected into the SdFFF system. Eluted samples are then monitored by a Spectra 100 ultra-violet light variable wavelength detector operated at a wavelength of 254 nm. In SdFFF, particle retention is related to particle size thus, particles of different sizes elute at different times. The intensity of ultra-violet light absorbed in the detector is measured as different particles elute and this provides a measure of the number of particles in the detector cell as a function of time. The corresponding variation of absorbed light intensity with time is then recorded and converted into a plot of absorbed light intensity vs. particle diameter, using SdFFF software operated on a Zeos International 386SX-16/8 PC computer. This plot is then proportional to the variation of numbers of particles of a particular size vs. particle size.

With this equipment and these procedures, polystyrene latex particle size distributions are measured at exit outlet $a$ and exit outlet $b$. The number of particles of a particular diameter which exit through outlet $a$ is denoted $M_a$, and the number of particles of a particular diameter which exit through outlet $b$ is denoted $M_b$. The ratios of the numbers of particles of a particular diameter exiting outlets $a$ and $b$, and the numbers of particles of the same diameter which entered the channel in the feed substream are then determined. For a specific particle diameter, these are denoted using $F_a$ and $F_b$, respectively, which are then evaluated using the equations given by

$$F_a = \frac{M_a}{M_a + M_b} \tag{4}$$

and

$$F_b = 1 - F_a. \tag{5}$$

Graphs of $F_a$ and $F_b$ vs. particle diameter, $d$, are referred to as retrieval plots or recovery plots.

Comparing variations of $F_a$ and $d$ for different experimental conditions provides a quantitative indication of the amount of mixing and entrainment in the channel. With nominal channel flow, particles smaller than diameter $d_0$ leave the channel through exit $a$. The $F_a$ vs. $d$ plot for these particles then represents stable, laminar, two-dimensional channel behavior. Larger differences between this plot and other retrieval plots, which produce lower $F_a$ values at a particular particle diameter, indicate greater deviations from nominal channel behavior.

*Micrographs*

Micrographs showing the polystyrene latex particles are obtained using a Hitachi S-450 scanning electron microscope located in the Biology Department of the University of Utah.

*Experimental conditions and procedure*

Table 1 gives a summary of the experimental conditions studied. The velocity of the feed substream for all tests is $2.54 \times 10^{-3}$ m s$^{-1}$. For a fixed $\Delta\rho$, the velocity of the carrier solution is altered to vary the Reynolds number from 1.1–5.6. Newly prepared feed and carrier solutions are then employed for each subsequent test condition at different values of $\Delta\rho$. All experiments are done at laboratory ambient temperature, which is usually approximately 24°C. Solution densities are measured at 24°C using an AP Paar Corp. DMA model 602 high precision density meter, which gives values accurate to the sixth significant digit after the decimal in kg m$^{-3}$.

## NUMERICAL PREDICTION SCHEME

To obtain local streamwise velocities at different transverse and streamwise locations in the channel $u(s', z)$, numerical flow simulations are conducted

Table 1. Flow conditions employed for experiments and FLUENT calculations

| $d_c$ ($\mu$m) | $\dot{V}(a')$ (ml min$^{-1}$) | $\dot{V}(b')$ (ml min$^{-1}$) | $\dot{V}(a)$ (ml min$^{-1}$) | $(\Delta\rho/\rho)\times10^4$ | $l'$ ($\mu$m) | $\Delta U$ (cm s$^{-1}$) | $Re$ | $Ri$ |
|---|---|---|---|---|---|---|---|---|
| 11.1 | 0.75 | 5 | 1.98 | 18.9 | 39.5 | 0.715 | 0.28 | 0.014 |
| | | | | 8.12 | | | | 0.0061 |
| | | | | 6.22 | | | | 0.0047 |
| | | | | 2.40 | | | | 0.0018 |
| 20.7 | 0.75 | 6.75 | 6 | 15.3 | 38.6 | 1.01 | 0.39 | 0.0057 |
| | | | | 10 | | | | 0.0037 |
| | | | | 6.22 | | | | 0.0023 |
| | | | | 2.40 | | | | 0.0009 |
| 25.7 | 0.75 | 11 | 9 | 30.8 | 36.3 | 1.72 | 0.624 | 0.0037 |
| | | | | 21.3 | | | | 0.0026 |
| | | | | 11.9 | | | | 0.0014 |
| | | | | 8.17 | | | | 0.001 |
| 29.8 | 0.75 | 16 | 12 | 77.8 | 33.3 | 2.56 | 0.852 | 0.0039 |
| | | | | 40.2 | | | | 0.0020 |
| | | | | 28.9 | | | | 0.0014 |
| | | | | 21.3 | | | | 0.0010 |
| 34.6 | 0.75 | 21 | 16 | 77.8 | 30.9 | 3.30 | 1.05 | 0.0020 |
| | | | | 59 | | | | 0.0015 |
| | | | | 47.7 | | | | 0.0012 |
| | | | | 40.3 | | | | 0.0010 |

using FLUENT software [20]. Distributions of $u(s', z)$ are needed for determination of the length scale $l'$, which is employed to estimate Reynolds numbers and Richardson numbers. This approach is necessitated by the extremely small size of the channel used for the experiments, which prohibits the insertion and use of any sort of probe for measurement of local streamwise velocity distributions.

In the FLUENT calculations, dimensions of the channel employed for the flow predictions is 1500 $\mu$m long and 635 $\mu$m thick. The inlet splitter plate employed is 400 $\mu$m long. The program uses an iterative finite differencing numerical procedure to solve the Navier–Stokes equation governing the fluid flow. As the channel breadth is much greater than the channel thickness, it is assumed that flow variations along the lateral direction are negligible in comparison to the variations along the transverse direction. Thus, the numerical flow simulations are two-dimensional. They are also carried out for all of the experimentally investigated flow conditions indicated in Table 1.

To simulate the conditions present in the experiments, the density difference present in the isothermal flow between the feed and carrier substreams must be modeled. However, FLUENT lacks the capability to exactly model our experimental conditions wherein temperature is constant and the two fluid substreams contain different amounts of suspended solid particles with different densities and/or viscosities. This software limitation is overcome by predicting the characteristics of the two substreams at different temperatures to give the same density levels employed in the experiments. The thermal conductivities of the fluids in the FLUENT calculations are determined by equating Prandtl numbers ($\eta c_p/k$) in the numerical calculations to experimental Schmidt numbers ($\eta/\rho D$).

## EXPERIMENTAL RESULTS AND DISCUSSION

### *Characterization of flow behavior*

Numerous investigators [9, 11, 21] employ the Richardson number to characterize aspects of stratified shear layers. The dimensionless Richardson number is also used in this study to quantify channel behavior. The form employed here is the ratio of the square of the natural convection velocity scale to the square of the forced convection velocity scale. Following Schowalter *et al.* [11], the Richardson number is then given by

$$Ri = \frac{(\Delta\rho/\bar{\rho})Gl'}{(\Delta U)^2} \tag{6}$$

where $G$ is the acceleration due to gravity.

All data in Table 1 are obtained for $\Delta\rho > 0$ and $\rho_f > \rho_c$, or $Ri > 0$, which correspond to unstable density gradient conditions within the channel. Larger positive Richardson numbers thus indicate larger normalized magnitudes of the difference in density, $\Delta\rho = (\rho_f - \rho_c)$, between the upper feed substream and the lower carrier substream. As positive Richardson number increases, global and local density gradients across the mixing layer thus become more unstable. Note that the $\Delta\rho$ density difference is normalized by $\Delta U$, the velocity difference between the two streams. Consequently, the Richardson number given by equation (6) can also be thought of as the normalized ratio of the density gradient (which drives the buoyancy instabilities) and the square of the overall velocity

gradient (which provides a shear mechanism to induce flow instabilities).

When $\rho_f < \rho_c$, stable density gradients are present across the mixing layer in the channel, $\Delta\rho < 0$, and the Richardson number is less than zero. One stable density gradient is investigated in this study (as a baseline data set) at a Richardson number of $-0.0045$.

The Reynolds number is also based on the length scale $l'$ and velocity difference $\Delta U$. It is given by

$$Re = \frac{\rho l' \Delta U}{\eta}. \tag{7}$$

In the present study, the Reynolds number is changed by altering $\Delta U$. Richardson numbers are altered by varying either $\Delta\rho$ or $\Delta U$. $\Delta\rho$ is varied using dissolved sucrose crystals, as mentioned, and $\Delta U$ is changed by altering the carrier substream velocity.

*Distributions of local streamwise velocity and length scale $l'$*

Profiles of the local streamwise velocity downstream of the inlet splitter plate are presented in Fig. 3. Numerically predicted values in the figure are presented at $x$ locations ranging from 423–1500 $\mu$m for $\dot{V}(a) = 9.0$ ml min$^{-1}$, $\dot{V}(b) = 2.75$ ml min$^{-1}$, $\dot{V}(a') = 0.75$ ml min$^{-1}$, and $\dot{V}(b') = 11.0$ ml min$^{-1}$, which correspond to $Re = 0.624$, $l' = 36.3$ $\mu$m, $d_c = 25.7$ $\mu$m. The development of the velocity profiles as the shear layer advects downstream is apparent. As momentum is diffused in the $z$ direction, the profiles with two local maxima change shape until a single maximum is present in each profile near the spanwise center of the channel.

The characteristic integral length scale $l'$ employed in the Richardson number and Reynolds number provides a measure of the vertical extent of the shear layer and the mixing which occurs across it [9, 11]. It is determined at a location $x = 460$ $\mu$m, or 60 $\mu$m downstream of the splitter plate (which is 400 $\mu$m long in the numerical field) because this is where the maximum $l'$ value is predicted. The length scale is estimated using an equation having the form

$$l' = \left(\frac{1}{\Delta U^2}\right)\int_{z_a}^{z_b} (u_c - u(z))(u(z) - u_f)\,dz \tag{8}$$

where $u(z)$ is the local streamwise velocity at different transverse locations just downstream of the splitter plate, and $u_c$ and $u_f$ represent the local maximum magnitudes of the velocity distributions in the carrier and feed substreams, respectively. The limits of the integral, $z_a$ and $z_b$, extend from one local velocity maximum to another. Equation (8) is similar in form to $l'$ equations by Koop and Browand [9] and Schowalter *et al.* [11].

Plots of the variation of normalized length scale $l'$ with velocity ratio $\dot{V}(a)/\dot{V}(a')$ and with Reynolds number are presented in Figs. 4 and 5, respectively. Data are given for the 635 $\mu$m thick channel, as well as for one which is 1.59 cm thick. In the latter case, a 0.318 cm thick splitter plate is used in the FLUENT calculations. In both figures, the length scales for the two channels, normalized by channel thickness, cover the same ranges of values. When results from the two channels are compared at the same $\dot{V}(a)/\dot{V}(a')$ or $Re$, important differences due to channel thickness $w$ are evident. These differences are due to different shear layer thicknesses and behavior which are tied to the splitter plate thickness and channel profile characteristics just upstream of the end of the splitter plate. Generally, Figs. 4 and 5 show decreasing $l'/w$ as either

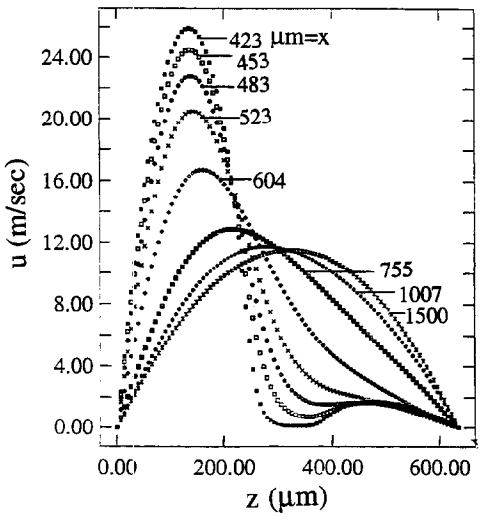


Fig. 3. Local streamwise velocity surveys from numerical simulations calculated at different streamwise locations downstream of the splitter plate for $Re = 0.624$, $l' = 36.3$ $\mu$m, $d_c = 25.7$ $\mu$m, $\dot{V}(a) = 9.0$ ml min$^{-1}$, $\dot{V}(b) = 2.75$ ml min$^{-1}$, $\dot{V}(a') = 0.75$ ml min$^{-1}$, and $\dot{V}(b') = 11.0$ ml min$^{-1}$.

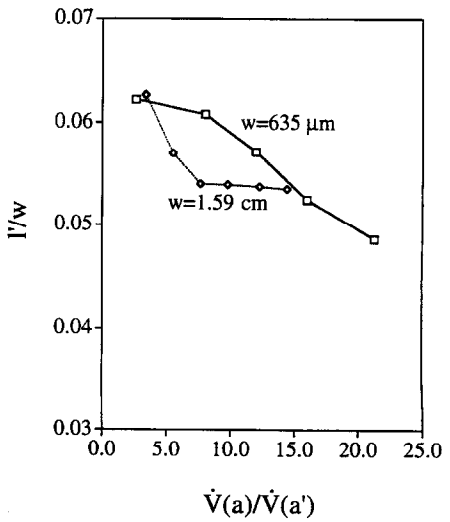


Fig. 4. Variation of normalized shear layer length scale with velocity ratio $\dot{V}(a)/\dot{V}(a')$ for a 635 $\mu$m thick channel and a 1.59 cm thick channel.

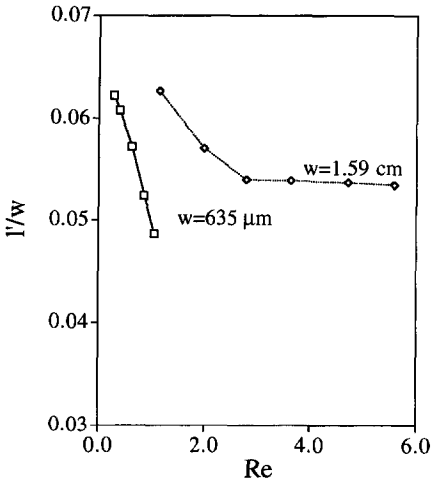


Fig. 5. Variation of normalized shear layer length scale with Reynolds number for a 635 $\mu$m thick channel and a 1.59 cm thick channel.

$\dot{V}(a)/\dot{V}(a')$ or $Re$ increase. Koop and Borwand [9] show how normalized magnitudes of $l'$ vary in a stratified shear layer for $250 < Re < 350$ and $0.05 < Ri < 0.20$.

*Retrieval plots and micrographs with stable and unstable channel flows*

A micrograph of the original polystyrene latex particle sample is presented in Fig. 6. The scale line just below the photograph is 50 $\mu$m long. By comparing this with the particles in the figure, particles with diameters ranging from 1–35 $\mu$m are evident.

After these particles are inserted into the channel feed substream, and then collected at the channel outlet $a$, retrieval plots such as the ones presented in Fig. 7 are obtained. To obtain these data, different density gradients are produced across the channel shear layer to give positive Richardson numbers (with unstable density gradients and $\Delta\rho > 0$) ranging from 0–+0.0037. In all cases, Reynolds number is 0.624, $\dot{V}(a') = 0.75$ ml min$^{-1}$, $\dot{V}(b') = 11.0$ ml min$^{-1}$, $\dot{V}(a) = 9.0$ ml min$^{-1}$, and $\dot{V}(b) = 2.75$ ml min$^{-1}$.

In each of the four parts of Fig. 7, the retrieval plot for a particular Richardson number greater than 0 (producing an unstable density gradient) is compared to the retrieval plot for a negative Richardson number of $-0.0045$. This latter case corresponds to a channel with a stable density gradient wherein $\rho_f < \rho_c$, as mentioned. As the Richardson number increases, differences between the retrieval plots for $Ri > 0$ and $Ri = -0.0045$ become greater. Thus, smaller percentages of particles with diameters smaller than $d_c$ are recovered through channel outlet $a$ as the Richardson number increases. Consequently, mixing and entrain-

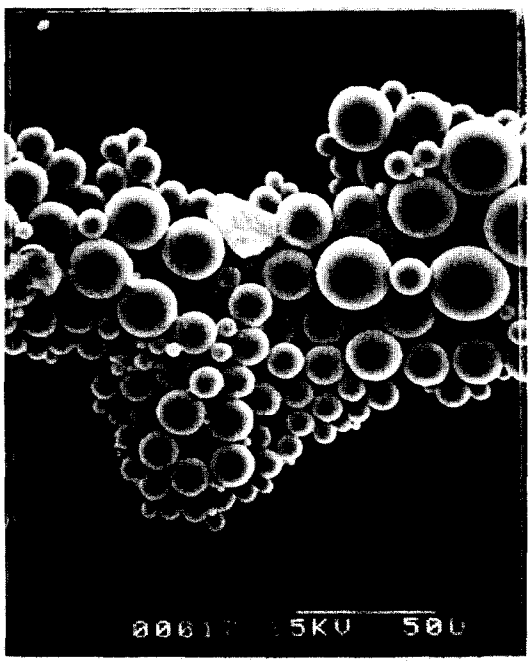


Fig. 6. Micrograph of the original polystyrene latex particle sample with diameters ranging from 1–35 $\mu$m.

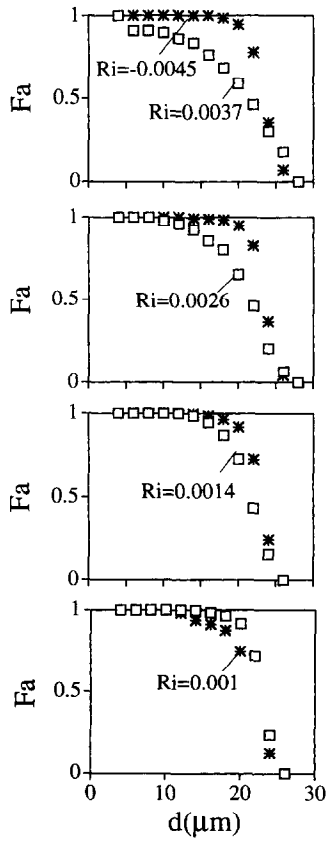


Fig. 7. Retrieval plots illustrating stable ($Ri = -0.0045$) and unstable ($Ri = +0.0010$, $+0.0014$, $+0.0026$, $+0.0037$) channel behavior for $Re = 0.624$, $d_c = 25.7$ $\mu$m, $l' = 36.3$ $\mu$m, $\dot{V}(a) = 9.0$ ml min$^{-1}$, $\dot{V}(b) = 2.75$ ml min$^{-1}$, $\dot{V}(a') = 0.75$ ml min$^{-1}$ and $\dot{V}(b') = 11.0$ ml min$^{-1}$.

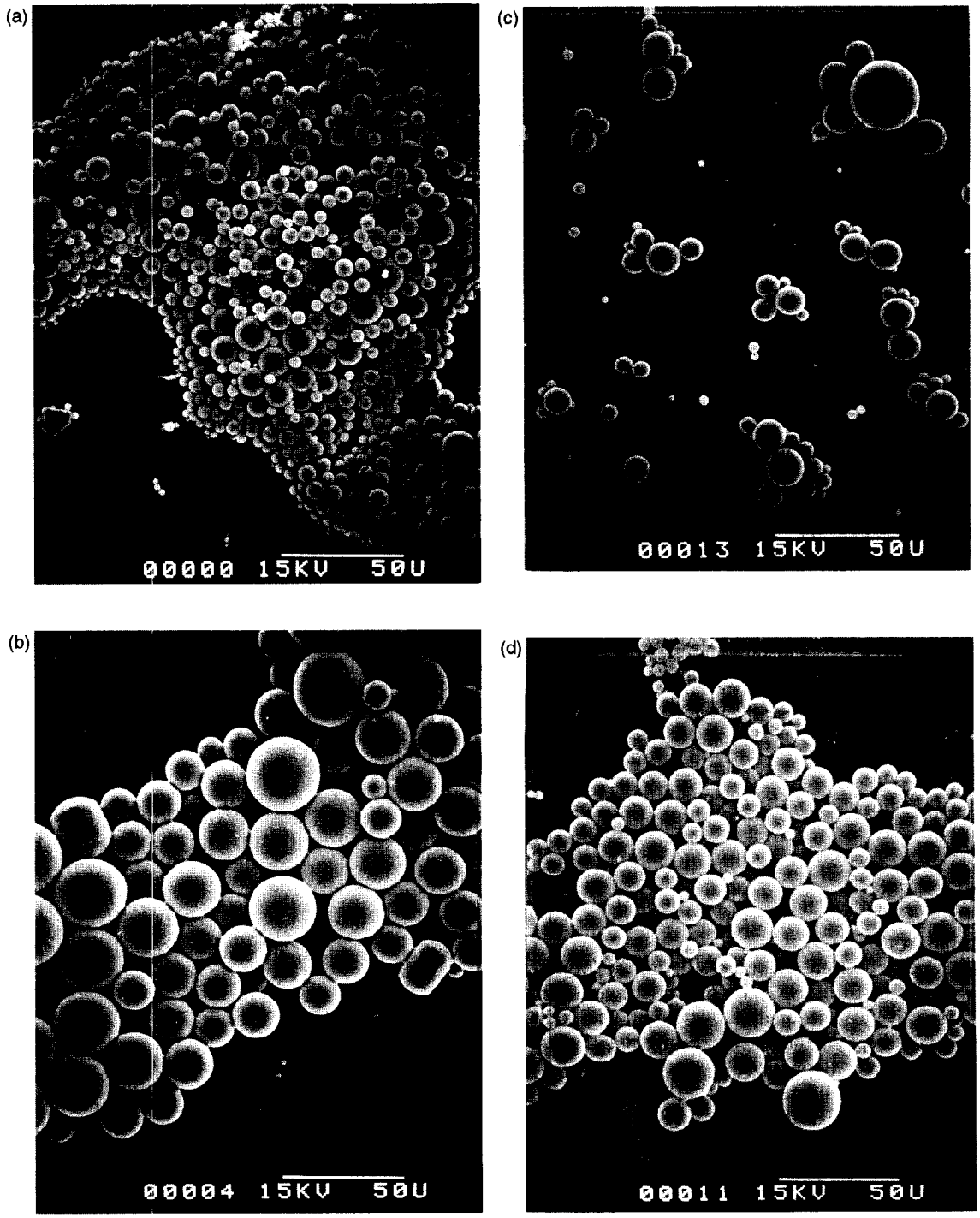


Fig. 8. Micrograph of the polystyrene latex particle samples taken from the exits of the channel for $Re = 0.39$, $l' = 38.6\ \mu m$, $d_c = 20.7\ \mu m$, $\dot{V}(a) = 6.0$ ml min$^{-1}$, $\dot{V}(b) = 1.5$ ml min$^{-1}$, $\dot{V}(a') = 0.75$ ml min$^{-1}$ and $\dot{V}(b') = 6.75$ ml min$^{-1}$. (a) $Ri = -0.0045$, stable channel flow, outlet $a$, (b) $Ri = -0.0045$, stable channel flow, outlet $b$, (c) $Ri = +0.0055$, unstable channel flow, outlet $a$, (d) $Ri = +0.0055$, unstable channel flow, outlet $b$.

ment become more important as the Richardson number increases.

This effect is also evident in the micrographs shown in Fig. 8. These are obtained for about the same experimental conditions as the results in Fig. 7. The size scale of the Fig. 8 photographs is the same as for the photographs in Fig. 6. Figure 8(a) shows the particles which emerge from outlet $a$, and Fig. 8(b) shows the

particles which emerge from outlet $b$ with $Ri = -0.0045$ and stable, two-dimensional, laminar flow in the channel. The two ranges of particle diameters in Figs. 8(a) and 8(b) are distinctly different from each other, and delineated approximately at the value of the cut-off diameter, $d_c$, given by equation (3), which is 20 $\mu$m. Particle diameters in Fig. 8(b) are consistently larger than 20 $\mu$m, and particle diameters in Fig. 8(a) are consistently smaller than 20 $\mu$m (considering the 50 $\mu$m scale below each photograph), which is entirely consistent with the theory for SF channels [17].

When the Richardson number is +0.0055, Fig. 8(c) for outlet $a$ and Fig. 8(d) for outlet $b$ show that all sizes of particles are present at each outlet. Such mixing is consistent with the results in Fig. 7. Experiments conducted at other flow conditions listed in Table 1 show similar qualitative trends.

*Mixing onset parameter* R

To identify the mixing onset boundary which demarcates flow dominant with and without substantial mixing in the channel, differences between the $Ri < 0$ retrieval plot and the $Ri > 0$ retrieval plots are quantified. This is done by evaluating the fractional difference between the areas under the retrieval plots obtained for outlet $a$, such as the ones shown in Fig. 7. Areas for stable and unstable density gradients are given by

$$A_{\text{stable}} = \int_{d_{\min}}^{d_{\max}} F_{a,\text{stable}}\, \mathrm{d}d \tag{9}$$

and

$$A_{\text{unstable}} = \int_{d_{\min}}^{d_{\max}} F_{a,\text{unstable}}\, \mathrm{d}d \tag{10}$$

respectively. Here, $d_{\max}$ and $d_{\min}$ are the largest and the smallest particle diameters in the feed sample, respectively. The quantitative magnitudes of each integral representing the area under an individual retrieval plot is obtained by numerical integration. The fractional difference denoted by mixing onset parameter $R$ then has the form

$$R = \frac{A_{\text{stable}} - A_{\text{unstable}}}{A_{\text{stable}}}. \tag{11}$$

$R$ thus provides a measure of the mixing and entrainment in the channel by indicating how different the $Ri > 0$ retrieval plot is from the $Ri = -0.0045$ retrieval plot. From equations (4), (9)–(11), $R$ variations are entirely due to the ratio of the number of polystyrene latex particles exiting outlet $a$ relative to the total number of polystyrene latex particles which enter the channel through the feed substream at inlet $a'$. As such, the particles act as tracers to indicate the amount of mixing and entrainment between the two fluid substreams in the channel. As mixing and entrainment increase, more particles of a particular diameter (less than $d_c$) are spread over the channel cross-section, fewer particles are present at outlet $a$, and the larger is the mixing onset parameter $R$. Higher $R$ are thus due to situations such as the ones illustrated in Figs. 8(c) and 8(d) wherein particles of all sizes (present in the original sample) exit both outlets $a$ and $b$.

The amount of this mixing is dependent upon the density difference between the carrier and feed substreams, as quantified by the Richardson number. The extent of density stratification influences thus seem to depend upon the Reynolds number, Richardson number, as well as other factors. The mixture of polystyrene latex particles and fluid as a two-phase flow may also have some influence. As such, the particles probably alter the variations of $R$ with $Ri$ and $\dot{V}(a)/\dot{V}(a')$ by small amounts compared to a single phase flow with no particles but the same density gradients.

To quantify the onset of mixing and entrainment in the present study, magnitudes of $R$ are determined for all flow conditions listed in Table 1 for different Richardson numbers and channel volumetric flow rates. The variation of $R$ as a function of Richardson number for different $\dot{V}(a)/\dot{V}(a')$ is shown in Fig. 9. As $Ri$ increases, a steep increase in $R$ is evident for each value of $\dot{V}(a)/\dot{V}(a')$. In addition, the slope of the $R$ vs. $Ri$ line increases as $\dot{V}(a)/\dot{V}(a')$ increases. This occurs

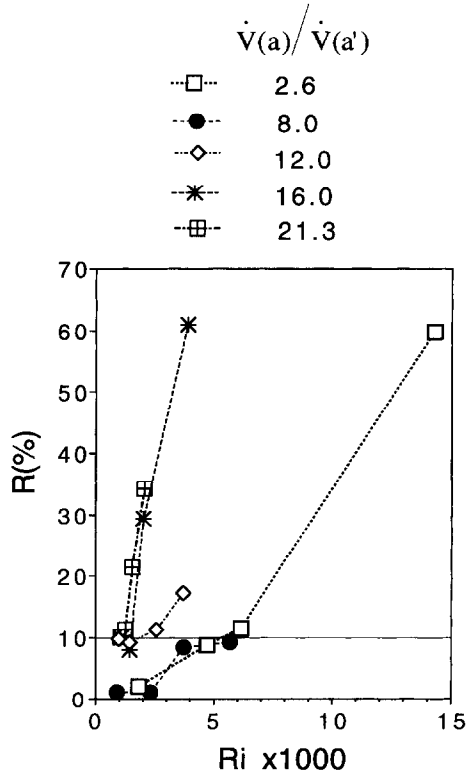


Fig. 9. Variation of mixing onset parameter $R$ with Richardson number for different values of the velocity ratio $\dot{V}(a)/\dot{V}(a')$.

because, as $\dot{V}(a)/\dot{V}(a')$ becomes larger, the laminar flow from inlet $a'$ is located more closely to wall $A$ (see Fig. 1(a)) as it is advected downstream. As a result, relatively larger fractions of polystyrene latex particles are located in a smaller channel volume locally just downstream of the splitter plate. Particles continue to be maintained in this fashion as they advect downstream until significant sedimentation begins to occur. A larger range of particle sizes are also present above the outlet splitter plane as $\dot{V}(a)/\dot{V}(a')$ increases. Consequently, more flow mixing occurs at a particular Richardson number than for situations where $\dot{V}(a)/\dot{V}(a')$ is less. The arrangements of different sized particles, which occur as $\dot{V}(a)/\dot{V}(a')$ increases, also augment $\Delta\rho$ gradients locally over very small volumes, even though the overall density gradient for the entire channel (on which the Richardson number is based) may be less.

*Mixing onset boundary of the stratified shear layer*

The mixing onset boundary is the range of experimental conditions which demarcates channel behavior with very little or no mixing and entrainment from channel behavior with significant mixing and entrainment. The former condition is considered to be present when $A_{\text{unstable}}$ is at least 90% of $A_{\text{stable}}$, which means that the difference in the areas of the stable and unstable retrieval plots is less than or equal to 10%. This occurs when 10% or less of particles with diameters less than $d_c$ do not leave the channel from exit $a$. In equation form, this corresponds to

$$R \leqslant 0.1. \tag{12}$$

The upper limit of equation (12) is identified in Fig. 9. Intersections of this $R = 0.1$ line with lines through experimental data at different $\dot{V}(a)/\dot{V}(a')$ in this figure thus locates corresponding critical Richardson numbers $Ri_{cr}$ on the mixing onset boundary. Critical Richardson numbers along this boundary thus vary with $Ri$ and $\dot{V}(a)/\dot{V}(a')$.

The variation of $Ri_{cr}$ with Reynolds number is shown in Fig. 10 for different values of $\dot{V}(a)/\dot{V}(a')$. Also included in the figure are symbols representing all measured data points. From this figure, it is evident that the line which indicates the mixing onset boundary is strongly dependent upon the Richardson number with a significantly weaker dependence on the Reynolds number. This provides some evidence that the instabilities in the channel are more a result of unstable density gradients than shear gradients. This conclusion is also supported by the range of Reynolds numbers of the present stratified shear layers, which are shown in Fig. 2 to be significantly less than ones employed in several other studies of mixing layers with globally stable stratification [7, 9, 11]. Consequently, the shear layers in our channel are significantly weaker than the shear layers of these other investigations. This brings up the question as to whether or not Kelvin–Helmholtz instabilities develop in our channel. If the

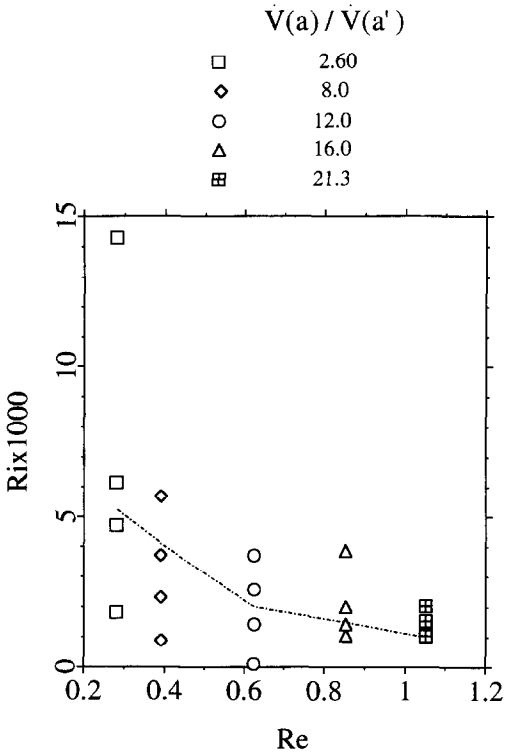


Fig. 10. Mixing onset boundary as dependent upon Richardson number and Reynolds number.

Kelvin–Helmholtz vortex structures do develop at Reynolds numbers less than two in our channel, they are probably triggered or initiated in some way by the disturbances induced by unstable density stratification. Alternatively, if the Kelvin–Helmholtz vortex structures ordinarily produced at higher Reynolds numbers are not present in our channel, then the observed mixing is induced by vortex structures which result from unstable density stratification alone [18].

As Reynolds number increases from 0.3–1.1 in Fig. 10, the critical Richardson number decreases from approximately +0.0055–+0.0010. This indicates that fluid particles are more likely to be mixed by density stratification between different flow laminate as shear in the mixing layer (as characterized by $\Delta U$) becomes more significant relative to the magnitude of kinematic viscosity. As Reynolds numbers become lower than 0.6, two-dimensional, stable, laminar flow with little or no mixing is present over a wider range of Richardson numbers.

Figure 11 provides additional information on the dependence of the mixing onset boundary on channel volumetric flow rates. Here, all experimental data points are located on $Ri$ vs. $\dot{V}(a)/\dot{V}(a')$ coordinates, and the mixing onset boundary corresponding to $R = 0.1$ is illustrated by a dotted/dashed line. Like the results in Fig. 10, the mixing onset boundary in Fig. 11 is strongly dependent upon the Richardson number with a significantly weaker dependence on channel

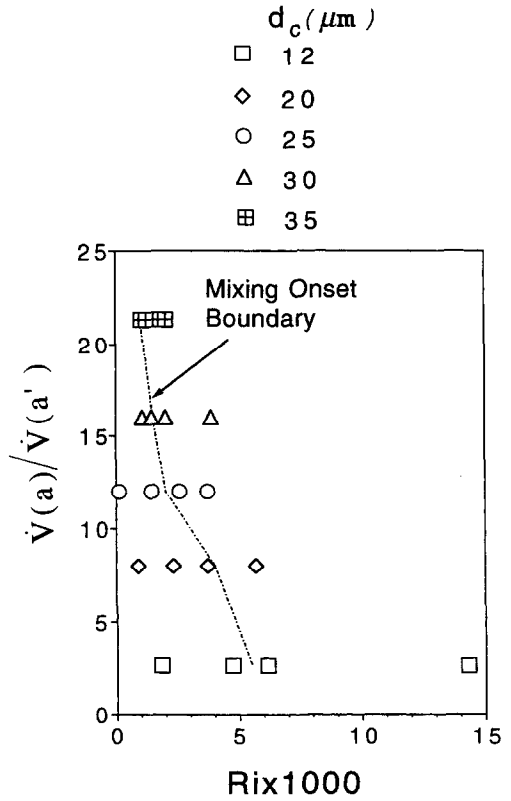


Fig. 11. Mixing onset boundary as dependent upon Richardson number and velocity ratio $\dot{V}(a)/\dot{V}(a')$. Symbol labels are same as for Fig. 10.

inertial forces characterized by the channel flow rate ratio $\dot{V}(a)/\dot{V}(a')$. As $\dot{V}(a)/\dot{V}(a')$ increases from 2.6–21.3, the critical Richardson number decreases from approximately $+0.0055$–$+0.0010$. This means that mixing is more likely to occur at a particular Richardson number as $\dot{V}(a)/\dot{V}(a')$ increases. The arrangements of particles of different sizes which occur as $\dot{V}(a)/\dot{V}(a')$ increases, mentioned earlier, are also important. This is particularly the case as a larger range of particle sizes are sustained above the channel outlet splitter plane, and as local density gradients in the channel are augmented. As the stratified shear layer advects further downstream, increasing amounts of sedimentation occur and more particles move in the transverse (i.e. $-z$) direction. As a result, both local and global density gradients decrease making the density across the channel more uniform.

Figures 10 and 11 both show that mixing is unlikely to be present in the channel when the positive Richardson number is less than $+0.0010$. Within this range of experimental conditions, stable, two-dimensional, laminar channel flow is maintained for all experimental conditions used in this study (in spite of the presence of globally unstable density gradients). Such behavior provides additional support for the two scenarios pertaining to Kelvin–Helmholtz instabilities, mentioned earlier, because it means that no mixing or any instability producing any mixing occurs at positive Richardson numbers near $Ri = 0$, regardless of the magnitude of the Reynolds number. Another interesting characteristic of the $Ri < +0.0010$ flows occurs when volumetric flow rates are adjusted so that particle cut-off diameter is 35 $\mu$m, which is the upper limit of range of particle sizes employed. With this situation, all polystyrene latex particles are nominally maintained above the outlet splitter plane all along their transit through the channel. Consequently, almost none of the particles exit the channel through outlet *b*.

## SUMMARY AND CONCLUSIONS

The mixing onset boundary due to unstable density stratification in the presence of a shear layer is examined in a thin, ribbon-like, 635 $\mu$m thick, rectangular channel at low Reynolds numbers ($Re < 2$). The effects of the mixing onset on mass transfer of solid particles in the channel are examined, especially as the flow deviates from two-dimensional, laminar, unmixed conditions.

The experimental conditions locating the mixing onset boundary are characterized using a newly defined mixing onset parameter $R$. This parameter depends upon the number and size distributions of polystyrene latex particles which leave the channel through two different exits. Thus, the polystyrene latex particles are used as flow tracers to give an indication of path line trajectories through the channel at different flow conditions. Flow mixing and entrainment, and disruptions to mass transfer mechanisms ordinarily providing good fractionation, are considered present when exiting particle size distributions are different from theoretically determined distributions [17] for two-dimensional, stable laminar mass transfer in the channel. This theory predicts a particle size cut-off diameter resulting from the gravitational cross field which approximately separates larger sized particles which normally leave the channel at the bottom exit from smaller sized particles which ordinarily leave the channel through the top exit.

The mixing onset boundary is characterized in terms of the Richardson number of which it is a strong function. The mixing onset boundary shows significantly less dependence upon the channel Reynolds number and the flow rate ratio $\dot{V}(a)/\dot{V}(a')$. In the experiments conducted, as $\dot{V}(a)/\dot{V}(a')$ increases from 2.6–21.3, or as the Reynolds number increases from 0.3–1.1, the critical Richardson number at the mixing onset boundary varies between $+0.0055$ and $+0.0010$. The mixing and entrainment observed in our study are thus believed to develop from instabilities which result more from unstable density gradients than shear gradients.

*Acknowledgements*—The authors acknowledge support for this project from NSF Grant No. CHE-9322472. Dr M.

N. Myers is also acknowledged for his assistance with the experimental apparatus and facilities.

## REFERENCES


1. Woods, J. D., Wave-induced shear instability in the summer thermocline. *Journal of Fluid Mechanics*, 1968, **32,** 791–800.
2. Orlanski, I. and Bryan, K., Formulation of the thermocline step structure by large amplitude internal gravity waves. *Journal of Geophysical Research*, 1969, **74,** 6975–6983.
3. Marmorino, G. O., Observations of small-scale mixing processes in the seasonal thermocline, part II: wave breaking. *Journal of Physical Oceanography*, 1987, **17,** 1348–1355.
4. Thorpe, S. A., Hall, A. J., Taylor, C. and Allen, J., Billows in Loch Ness. *Deep-Sea Research*, 1977, **24,** 371–379.
5. Farmer, D. M. and Armi, L., The flow of Atlantic water through the Straight of Gibraltar. *Progress in Oceanography*, 1988, **21,** 1–8.
6. Brown, G. L. and Roshko, A., On density effects and large structure in turbulent mixing layers. *Journal of Fluid Mechanics*, 1974, **64,** 775–816.
7. Browand, F. K. and Winant, C. D., Laboratory observations of shear-layer instability in a stratified fluid. *Boundary Layer Meterology*, 1973, **5,** 67–77.
8. Patnaik, P. C., Sherman, F. S. and Corcos, G. M., A numerical simulation of Kelvin–Helmholtz waves of finite amplitude. *Journal of Fluid Mechanics*, 1976, **73,** 215–240.
9. Koop, C. G. and Browand, F. K., Instability and turbulence in a stratified fluid with shear. *Journal of Fluid Mechanics*, 1979, **93,** 135–159.
10. Klassen, G. P. and Peltier, W. R., The influence of stratification on secondary instability in free shear layers. *Journal of Fluid Mechanics*, 1991, **227,** 71–106.
11. Schowalter, D. S., Van Atta, C. W. and Lasheras, J. C., A study of streamwise vortex structure in a stratified shear layer. *Journal of Fluid Mechanics*, 1994, **281,** 247–291.
12. Komori, S., Kanzaki, T. and Murakami, Y., Simultaneous measurements of instantaneous concentrations of two species being mixed in a turbulent flow by using a combined laser-induced fluorescence and laser-scattering technique. *Physics of Fluids A*, 1989, **1**(2), 349–352.
13. Komori, S., Hunt, J. C. R., Kanzaki, T. and Murakami, Y., The effects of turbulent mixing on the correlation between two species and on concentration fluctuations in non-premixed reacting flows. *Journal of Fluid Mechanics*, 1991, **228,** 629–659.
14. Nagata, K. and Komori, S., Heat and mass transfer in strong stable stratification. *Transactions of the Japan Society of Mechanical Engineers B*, 1995, **61**(586), 2197–2205.
15. Nagata, K. and Komori, S., Direct numerical simulation of the Prandtl number effects on the counter-gradient scalar transfer in strong stable stratification. *Transactions of the Japan Society of Mechanical Engineers B*, 1996, **62**(600), 3142–3148.
16. Komori, S. and Nagata, K., Effects of molecular diffusivities on counter-gradient scalar and momentum transfer in strong stable stratification. *Journal of Fluid Mechanics*, 1996, **326,** 205–237.
17. Giddings, J. C., Optimization of transport-driven Continuous SPLITT Fraction. *Separation Science and Technology*, 1992, **27,** 1489–1504.
18. Gupta, S., Investigation of resolution deteriorating factors and new applications in Continuous SPLITT Fractionation. Ph.D. thesis, University of Utah, Salt Lake City, Utah, 1997.
19. Giddings, J. C., Moon, M. H., Williams, P. S. and Myers, M. N., Particle size distribution by sedimentation/steric FFF: development of a calibration procedure based on density compensation. *Analytical Chemistry*, 1991, **63,** 1366–1372.
20. FLUENT (V4), Version 4.2, Fluent Inc., Lebanon, New Hampshire, 1993.
21. Cardoso, S. S. and Woods, A. W., On convection and mixing driven by sedimentation. *Journal of Fluid Mechanics*, 1995, **285,** 165–180.